Jinst

Published by IOP Publishing for Sissa Medialab

Received: *December 12, 2016*
Revised: *January 12, 2017*
Accepted: *February 5, 2017*
Published: *???, 2017*

14th Topical Seminar on Innovative Particle and Radiation Detectors
3–6 October 2016
Siena, Italy

Ultra-Fast Silicon Detectors for 4D tracking

V. Sola,[1][a,1] R. Arcidiacono,[a,c] A. Bellora,[b] N. Cartiglia,[a] F. Cenna,[a,b] R. Cirio,[a,b] S. Durando,[b] M. Ferrero,[a,b] Z. Galloway,[d] B. Gruey,[d] P. Freeman,[d] M. Mashayekhi,[e] M. Mandurrino,[a] V. Monaco,[a,b] R. Mulargia,[a,b] M.M. Obertino,[a,b] F. Ravera,[a,b] R. Sacchi,[a,b] H.F-W.Sadrozinski,[d] A. Seiden,[d] N. Spencer,[d] A. Staiano,[a] M. Wilder,[d] N. Woods[d] and A. Zatserklyaniy[d]

[a] *INFN Sezione di Torino, Torino, Italy*
[b] *Università di Torino, Torino, Italy*
[c] *Università del Piemonte Orientale, Novara, Italy*
[d] *Santa Cruz Institute for Particle Physics, UC Santa Cruz, CA, U.S.A.*
[e] *Hakim Sabzevari University, Sabzevar, Iran*

E-mail: valentina.sola@to.infn.it

Abstract: We review the progress toward the development of a novel type of silicon detectors suited for tracking with a picosecond timing resolution, the so called Ultra-Fast Silicon Detectors. The goal is to create a new family of particle detectors merging excellent position and timing resolution with GHz counting capabilities, very low material budget, radiation resistance, fine granularity, low power, insensitivity to magnetic field, and affordability. We aim to achieve concurrent precisions of ~ 10 ps and ~ 10 μm with a 50 μm thick sensor. Ultra-Fast Silicon Detectors are based on the concept of Low-Gain Avalanche Detectors, which are silicon detectors with an internal multiplication mechanism so that they generate a signal which is factor ~ 10 larger than standard silicon detectors.

Keywords: Timing detectors; Particle tracking detectors (Solid-state detectors)

[1]Corresponding author

doi:xxxxxxx

Contents

1 Setting the stage

A recent development in silicon detector technology is the capability of adding low controlled gain into an otherwise standard silicon sensor [1]. This new type of silicon sensors, the so called Low-Gain Avalanche Diodes (LGAD), promises to enhance significantly the capability to measure track arrival times, leading to a dramatic improvement in the capability of silicon arrays. The goal is to maintain simultaneously the high granularity for spatial measurement and the capability for high rate data collection while making very accurate time measurements [2]. In fact the time measurement requires very short duration signals allowing for even larger data rates than conventional silicon sensors. Not all sensors geometries, thicknesses or gain values are suitable for precise timing measurements: we call Ultra-Fast Silicon Detectors (UFSD) those LGAD sensors optimized for timing measurements [3].

2 The effect of timing information

The inclusion of timing information in the structure of a recorded event has the capability of changing the way we design experiments, as this added dimension dramatically improves the reconstruction process, as reported in [4].

Depending on the type of detector design that will be pursued, timing information can be available at different stages in the reconstruction of an event. The most complete option is that

timing information is associated to each point of the track, bringing a simplification already in the reconstruction algorithm, where only time-compatible hits are used in the pattern recognition phase. However, in this case the electronics is very demanding, as it needs to be able to accurately measure the time of the hit on each pixel in the tracker detector. This option is indeed quite difficult to achieve, due to the massive increase of power consumption that such architecture would require. This increase in power consumption can be avoided by reducing the extension and granularity of the timing information, moving the timing sensors outside the volume of the tracker. This option allows to assign timing information to each reconstructed track without changing the the vast majority of the tracker hardware and instrumenting a dedicated "timing detector". This specific idea has been explored by ATLAS [5] in order to improve Level 1 trigger decision and in the CMS upgrade [6].

Considering a specific situation, at the HL-LHC [7] the number of events per bunch crossing will be of the order of 150–200, with an average distance between vertices of 500 μm and a timing rms spread of 150 ps. Considering a vertex separation resolution of 250–300 μm along the beam direction (present resolution for CMS and ATLAS), there will be 10-15% of reconstructed vertices composed by two events. Without the possibility to separate these events using timing information, this overlap will cause a degradation in the precision of the reconstructed variables, and lead to loss of overall efficiency. We can therefore conclude that accurate timing information at the HL-LHC will allow to exploit the full luminosity delivered by the machine.

3 Time-tagging detectors

Figure 1 shows the main components of a sensor and its associated electronics able to tag the arrival time of a particle (a time-tagging detector). For a pioneering article on timing see [8] while for an up-to-date review of current trends in electronics see [9]. The sensor, shown as a capacitor (C_d) with a current source in parallel, is read-out by a pre-amplifier that shapes the signal. The pre-amplifier output is then compared to a fixed threshold to determine the time of arrival. In the following we will use this simplified model and we will not consider more complex and space-consuming approaches such as waveform sampling. Note that averaging multiple (N) measurements at different threshold values does not lead to an improvement in the time resolution proportional to $1/\sqrt{N}$ since the points are strongly correlated.

In the model shown in figure 1, the particle arrival time is defined as the instant t_0 when the signal goes over the threshold (V_{th}): every effect that changes the shape of the signal in the vicinity of the value V_{th} causes t_0 to move either earlier or later and therefore affects the time resolution, σ_t. There are several effects that influence the total value of the time resolution: (i) the TDC binning, (ii) the Landau amplitude variation (Time Walk), (iii) the electronic noise (Jitter), (iv) the Landau non uniform charge deposition (Landau noise), (v) the non uniform drift velocity and weighting field effects (Signal distortion):

$$\sigma_t^2 = \sigma_{\text{TDC}}^2 + \sigma_{\text{Time walk}}^2 + \sigma_{\text{Jitter}}^2 + \sigma_{\text{Landau noise}}^2 + \sigma_{\text{Signal distortion}}^2 \,. \tag{3.1}$$

In the following a detailed explanation of each term is given:

(i) The contribution of the TDC term can be neglected, as thanks to the fine binning of the TDCs commonly in use in high energy physics experiments (as for e.g. the HPTDC [10]), σ_{TDC} can be kept below 10 ps.

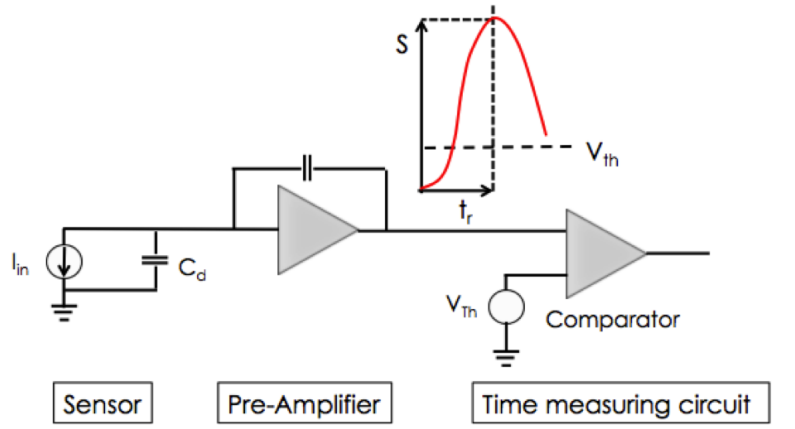

Figure 1. Main components of a detectors able to tag the arrival time of a particle. The time is measured when the signal crosses the comparator threshold V_{th}.

(ii) The effect of the time walk can be compensated by means of an appropriate electronic circuit (either Constant Fraction Discriminator or Time over Threshold). Under this assumption, the effect of Landau variation in signal amplitude are compensated, but not that of shape variation.

(iii) The jitter term represents the time uncertainty caused by the early or late firing of the comparator due to the presence of noise. It is directly proportional to the noise N and is inversely proportional to the slope of the signal around the value of the comparator threshold. Assuming a constant slope we can write $dV/dt = S/t_r$ (see figure 1) and therefore:

$$\sigma_{\text{Jitter}} = \frac{N}{dV/dt} = \frac{t_r}{S/N} \,. \tag{3.2}$$

(iv) The ultimate limit to signal uniformity is given by the physics governing energy deposition: the charge distribution created by an ionizing particle crossing a sensor varies on an event-by-event basis. These variations not only produce an overall change in signal magnitude, which is at the root of the time walk effect (ii), but also produce an irregular current signal (Landau noise). Figure 2 (left) shows two examples of the simulated[1] energy deposition by a minimum ionizing particle, while figure 2 (right) shows the associated generated current signals and their components. The variations are rather large and they can severely degrade the achievable time resolution. There are two ways to mitigate this effect: integrating the output current over times longer than the typical spike length and using thin sensors, as their steeper signal is more immune to signal fluctuations; the intrinsic limit of $\sigma_{\text{Landau noise}}$ is $\sim 20\,\text{ps}$ and constitutes the dominant factor to the overall time resolution for the sensor (for more details see [12]).

[1]All the simulations presented in this document are performed using Weightfield2 (WF2), an open source program available at cern.ch/nicolo,WF2

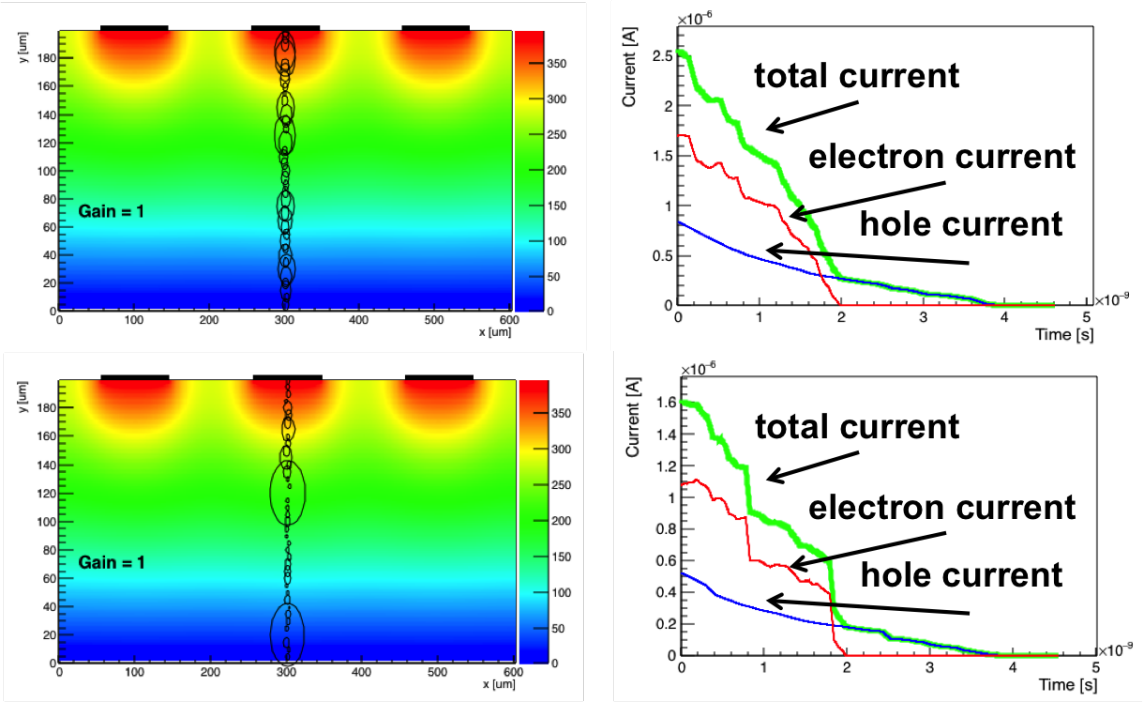

Figure 2. Energy deposits in a silicon detector with gain = 1 (left), and the corresponding current signals (right).

(v) In every particle detector, the shape of the induced current signal can be calculated using the Shockley-Ramo [13, 14] theorem that states that the current induced by a charge carrier is proportional to its electric charge q, the drift velocity v and the weighting field E_w:

$$i = -q\,\vec{v}\cdot\vec{E_w}\ . \tag{3.3}$$

This equation points out the key points in the design of sensors for accurate timing. First, the drift velocity needs to be constant throughout the volume of the sensor. Non-uniform drift velocities induce variations in signal shape as a function of the hit position, as shown in figure 3 a), spoiling the overall time resolution. The easiest way to obtain uniform drift velocity throughout the sensor is to have an electric field high enough to move the carriers with saturated drift velocity, v_{sat}. Second, the sensors need to have a width very similar to the pitch, and larger than the sensor thickness, d: width $\sim$ pitch $\gg$ thickness. These requirements are making the weighting field very uniform along the sensor width, as shown in figure 3 b).

The integration of time-tagging capabilities into a position sensor produces a steep increase in system complexity. Part of this complexity can be addressed by smart architectures, new technological nodes (for example 65 nm) allowing higher circuit densities and new chip designs. However the present bottlenecks inherent to hybrid systems, having sensors and electronics built on separated substrates, will ultimately limit the complexity and drive the cost. Most likely the real turning point of 4D tracking will happen when monolithic technology will be mature enough to allow integrating the sensor and the electronics in the same substrate, reducing interconnections and keeping the capacitance of each sensor low. As we are deciding now (2016) the choices for

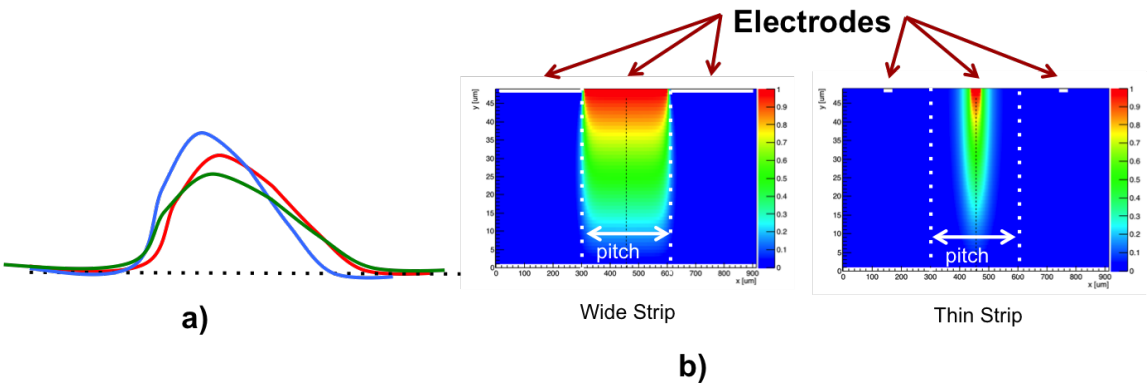

Figure 3. a) The signal shape depends on the velocity of the electron-hole pairs generated by the impinging particle: in case of non-saturated drift velocity, the output signal will depend on the impinging position. b) Weighting field for two configurations: wide strip (left), and thin strip (right). In thin strips, the weighting field is such that particles hitting near the center of the strip generate a much steeper and earlier signal.

HL-LHC (2025), this evolution will not be used at HL-LHC, but it will probably appear first in smaller experiments, and then be used on larger scales.

4 Design of a 4D tracker using Ultra-Fast Silicon Detectors

4.1 Low-Gain Avalanche Diodes

Standard silicon detectors can be used in timing applications, provided the sensor geometry is appropriate. Currently, the NA62 experiment [15] is employing a track-timing detector, the so called Gigatracker, that uses 200 μm thick sensors with $300 \times 300\ \mu m^2$ pixels. The expected time resolution is $\sigma_t \sim 150$ ps. Recently [16], employing an extremely low noise new circuit, a resolution of $\sigma_t \sim 105$ ps has been reached using a 100 μm thick, $2 \times 2\ mm^2$ pad sensor. Standard silicon sensors have therefore the capability of reaching good time resolutions, it is rather difficult to reach resolutions better than $\sigma_t \sim$ 80–100 ps given their small signal. The natural evolution of this problem is therefore to manufacture silicon sensors with a larger output signal: the Low-Gain Avalanche Diodes (LGAD).

LGAD is a new concept in silicon detector design, merging the best characteristics of standard silicon sensors with the main feature of APD [17–21], however without the additional problems affecting high gain devices (SiPM and APD). A SiPM sensor is a collection of many small pixels working in Geiger mode, and it needs several pixel cells to fire at the same time in order to have a large signal: since an impinging particle fires a single pixel, the SiPM signal from a MIP is too small to be used efficiently. APD, given their high gain, produce a very large signal in response to a MIP particle, ideal for timing, however they are difficult to segment, and their high gain, as explained in section 4.3, makes them very noisy as soon as the leakage current increases.

Charge multiplication in silicon sensors happens when the charge carriers are in electric fields of the order of $E \sim 300$ kV/cm. Under this condition the electrons (and to less extent the holes) acquire sufficient kinetic energy to generate additional e/h pairs. A field value of 300 kV/cm can be obtained by implanting an appropriate charge density that locally generates very high fields

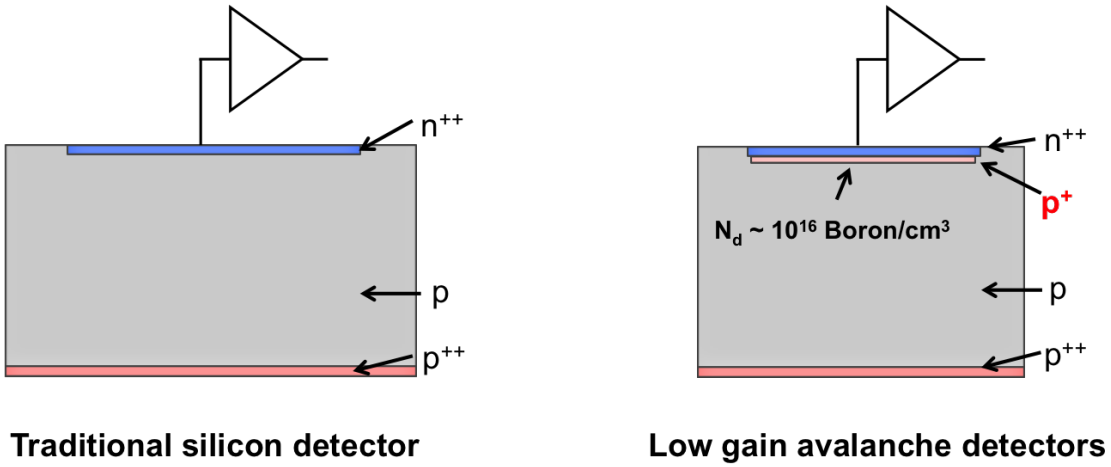

Figure 4. Schematic of a traditional silicon diode (left) and of a Low-Gain Avalanche Diode (right). The additional p^+ layer underneath the n^{++} electrode creates, when depleted, a large local electric field that generates charge multiplications.

($N_D \sim 10^{16}/\text{cm}^3$). The gain has an exponential dependence on the electric field, according to the exponential law

$$N(x) = N_0\, G = N_0\, e^{\alpha(E)x}\,, \tag{4.1}$$

where x is the path length inside the high field region and $\alpha(E)$ is the impact ionisation rate, which is a strong function of the electric field. The additional doping layer present at the $n-p$ junction in the LGAD design, figure 4 (right), generates the high field necessary to achieve charge multiplication.

LGAD have the potentiality of replacing standard silicon sensors in almost every application, with the added advantage of having a large signal dV/dt and therefore being able to measure time accurately. Ultra-Fast Silicon Detectors are LGAD sensors optimized for timing performances.

4.2 The effect of charge multiplication

Using WF2 we can simulate the output signal of UFSD sensors as a function of several parameters, such as the gain value, sensor thickness, electrode segmentation, and external electric field. Figure 5 shows the simulated current, and its separate components, for a 50 μm thick detector. The initial electrons (red), drifting toward the n++ electrode, go through the gain layer and generate additional e/h pairs. The gain electrons (violet) are readily absorbed by the cathode while the gain holes (light blue) drift toward the anode and generate a large current.

The gain dramatically increases the signal amplitude, producing a much higher slew rate. Using again Ramo's theorem and assuming 75 e/h pairs produced per μm, the current induced by the secondary charges is given by:

$$di_{\text{Gain}} = dN_{\text{Gain}}\, q\, v_{\text{sat}} \frac{1}{d} = 75\, q\, v_{\text{sat}} \frac{G}{d}\, dt, \tag{4.2}$$

which leads to the following expression for the current slew rate:

$$\frac{di_{\text{Gain}}}{dt} = 75\, q\, v_{\text{sat}} \frac{G}{d}\,. \tag{4.3}$$

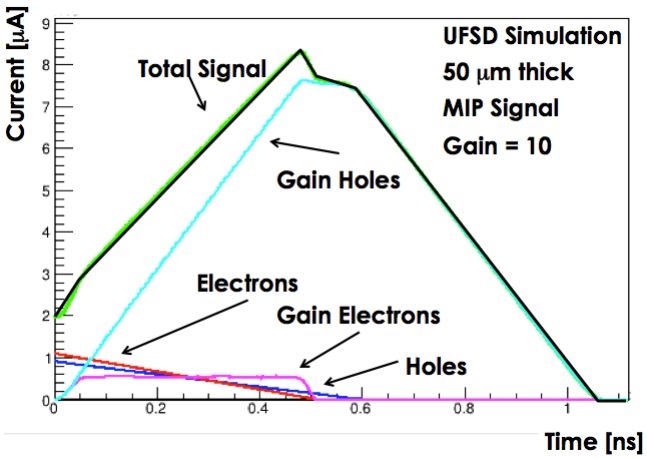

Figure 5. UFSD simulated current signal for a 50 μm thick detector. The evolution of the signal is governed by the initial electrons reaching the multiplication layer and generating the gain electrons and gain holes. The gain electrons are immediately absorbed by the n^{++} electrode, and therefore their contribution to the current in negligible. The gain holes, on the contrary, drifting towards the p^{++} contact, generate a large current with a large slew rate.

The current slew rate increase due to the gain mechanism is proportional to the ratio of the gain value over the sensor thickness (G/d), therefore thin detectors with high gain provide the best time resolution. Specifically, assuming a geometry with electrodes much larger than their separation, the maximum signal amplitude is controlled only by the gain value, while the signal rise time only by the sensor thickness, figure 6 (left).

Using WF2 we have cross-checked this prediction simulating the slew rate for different sensors thicknesses and gains, as shown in figure 6 (right): the slew rate in thick LGAD sensors, 200 and 300 μm, is a factor of $\sim$ 2 higher than that of traditional sensors, while in thin detectors, 50 and 100 μm thick, the slew rate is 5–6 times larger.

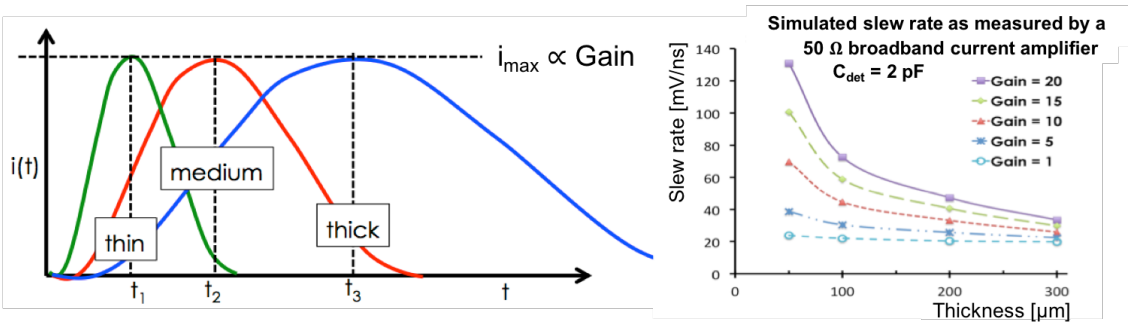

Figure 6. Left: in UFSD the maximum signal amplitude depends only on the gain value, while the signal rise time only on the sensor thickness; sensors of 3 different thicknesses (thin, medium, thick) with the same gain have signals with the same amplitude but with different rise time. Right: simulated UFSD slew rate as a function of gain and sensor thickness. Thin sensors with even moderate gain (10–20) achieve a much larger slew rate than traditional sensors (gain = 1).

4.3 Shot Noise in UFSD sensors

Shot noise arises when charge carriers cross a potential barrier, as it happens in silicon sensors. In sensors such as UFSD or APD this effect is enhanced by the gain and for this reason shot noise can be the dominant source of noise. As shown in figure 7 a), the sensor leakage current is the sum of two components: (i) surface current, that does not go through the multiplication layer, and (ii) bulk current, that is multiplied by the gain mechanism.

When carriers undergo multiplication, there is an additional mechanism that enhances shot noise: multiplication is a statistical process, therefore some carriers multiply more than others, causing an increase in noise, the so called *excess noise factor* (ENF). This effect is in addition to the increase in noise due to the gain value that simply multiplies the leakage current. ENF causes a very peculiar effect: in devices with gain, as the gain increases the ratio signal/noise (S/N) becomes smaller since shot noise increases faster than the signal, figure 7 b). In order to obtain a beneficial effect from the gain mechanism it is therefore necessary to have a gain value small enough (gain ≤ 20) that the signal increases while the noise increment is small enough to be in the shadow of the electronic noise floor. Shot noise is normally smaller than the electronic noise floor for unirradiated sensors, but it can become the dominant source of noise for irradiated detectors. Figure 8 shows the value of shot noise for a 4 mm^2, 50 μm thick silicon sensor, assuming a 2 ns long integration time as a function of fluence. In the plots the electronic noise is assumed to be $\sim 500\, e^-$ (ENC). Figure 8 a) demonstrates the dramatic effect of gain on shot noise, whereas in figure 8 b) is shown the effect of temperature (leakage current increases a factor of 2 every 7 degrees).

Figure 8 demonstrates that shot noise can become the most important source of noise for irradiated sensors with gain, and suggests that low gain and low temperature can keep this effect under control. Additionally, shot noise can be kept under control by keeping the volume under each each pixel/strip small, as the leakage current depends on the volume per electrode: $I_{Leak} = \alpha\, \Phi\, V$, with $\alpha = 3 \cdot 10^{-17}$/cm and Φ the particle fluence in n_{eq}/cm^2.

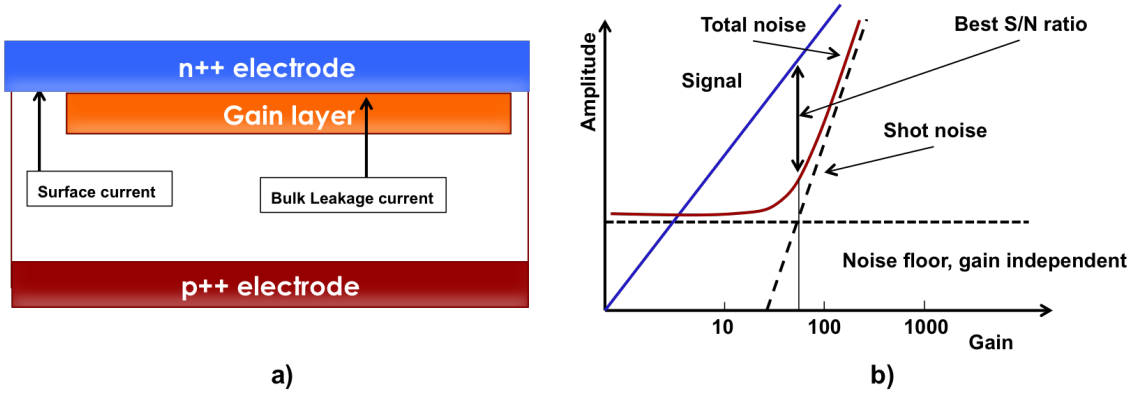

Figure 7. a) Sketch of the shot noise mechanism in sensors with internal gain: bulk current is multiplied by the gain, while surface current is not. b) Dependance of the current and noise amplitude as a function of gain: the signal increases linearly with gain while the noise at first is constant, and then increases faster than the signal when Shot noise becomes the dominant contribution [22].

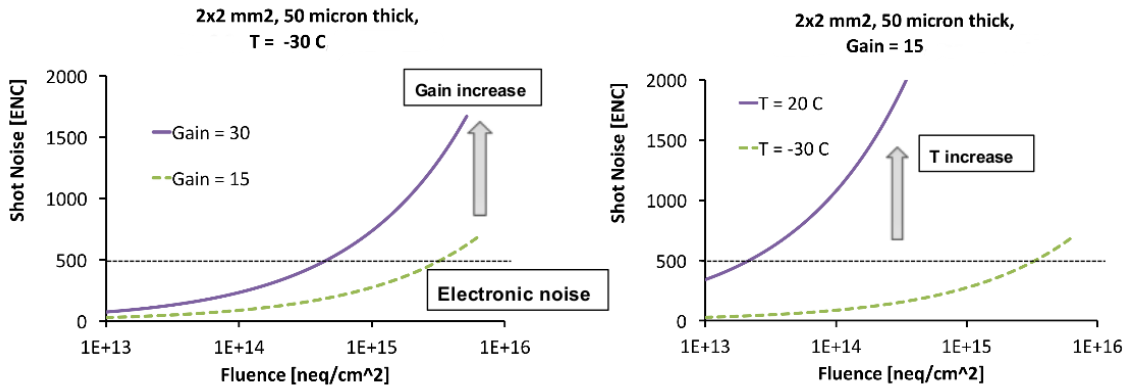

Figure 8. a) Shot noise increase as a function of fluence for two different gain values. b) Shot noise increase as a function of fluence for two different temperature values.

4.4 Temperature effects in UFSD sensors

The internal gain of a LGAD is influenced by the temperature by means of the carriers saturated velocity [23] and the impact ionisation rate introduced in eq. (4.1), which is related to the reciprocal of the mean free path of the carriers [24]. The study of the temperature dependence on the sensor performance is therefore crucial to calibrate and operate the devices at low temperatures, as requested by some of the major experiments.

Four different models for the impact ionisation rate as a function of the temperature have been implemented in WF2 and compared to data [25]. The *van Overtraeten* [26] and *Massey* [27] models are based on different parametrisations of the Chynoweth law [28]:

$$\alpha_{e,h}(E) = \gamma\, \alpha_{e,h,\infty}\, e^{-\frac{\gamma \beta_{e,h}}{|E|}}, \tag{4.4}$$

where $\alpha_{e,h,\infty}$ and $\beta_{e,h}$ are parameters assuming different values for electrons and holes and γ is a parameter independent from the charge carrier nature, while the *Bologna* [29] and *Okuto* [30] models propose their own law for $\alpha_{e,h}$. It is important to stress that all the models are empirical, therefore their parameters have been determined by fitting experimental data and are applied as reported in the litterature, without attempting any tuning. They are applicable for electric fields of the order of 100 kV/cm and temperatures around 300 K.

As shown in figure 9, the experimental data appear to be in a far better agreement with the *Massey* and the *Okuto* models, predicting a milder increase of the gain at low temperatures with respect to the *van Overstraeten* and *Bologna* model expectations. A good understanding of the LGAD behaviour as a function of the temperature is crucial, as changes in the gain value affect also the breakdown voltage point and the time resolution of the detector.

4.5 Radiation effects in UFSD sensors

Radiation damage causes three main effects: (i) decrease of charge collection efficiency, (ii) increase of leakage current, and (iii) changes in doping concentration.

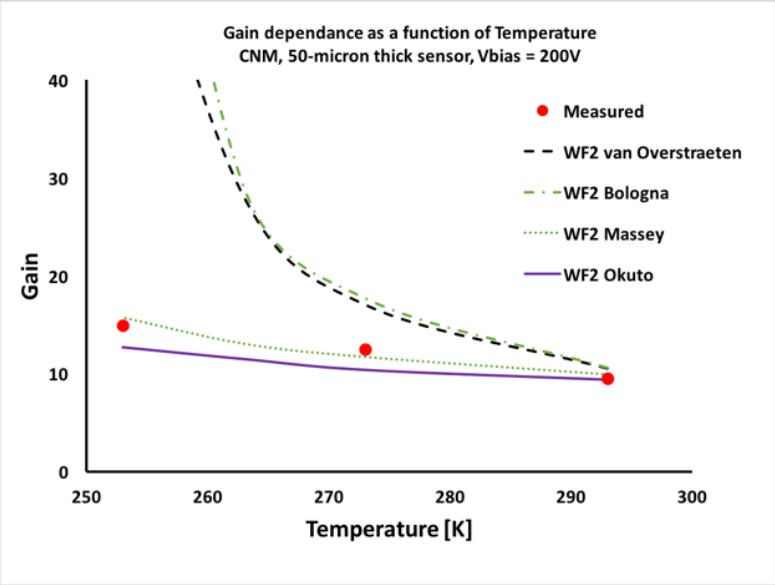

Figure 9. Gain as a function of temperature compared with WF2 simulations for a 50 μm thick LGAD.

Decrease of charge collection efficiency. Charge collection efficiency (CCE) measures the fraction of charge carriers that are not trapped by lattice defects. This fraction decreases with increasing radiation levels (with differences depending on the type of silicon and type of irradiation) and with increasing drift length. For irradiation levels around 10^{15} n_{eq}/cm^2, the mean free path in silicon is around 50 μm. Figure 10 shows the simulated [31] signal changes as a function of radiation level for a 50 μm thick sensor: the effect is rather small up to a fluence of 10^{15} n_{eq}/cm^2, and it becomes important above a fluence of $5 \cdot 10^{15}$ n_{eq}/cm^2. Interestingly, the initial edge of the signal, used for timing, it is not affected much.

Increase of leakage current. An increase in leakage current causes two important effects: (i) a larger noise, as explained in section 4.3, and (ii) a change in the apparent doping concentration. This second effect can be quite important, and it is presently under intense study.

Changes in doping concentration. UFSD sensors have shown a decrease of gain values for fluences above 10^{14} n_{eq}/cm^2, with a complete disappearance of the gain at 10^{15} n_{eq}/cm^2. This effect has not been understood yet, but there are two possible explanations: (i) an inactivation of acceptors due to radiation defects [32], and (ii) a dynamic reduction of the gain layer doping due to charge trapping. There are currently three research paths in the investigation of gain reduction, aiming at establishing a radiation hard design for UFSD [33]: (i) change the dopant of the p-type gain layer from Boron to Gallium, as Gallium, given its higher mass, has been shown to be less prone to become electrically inactive due to interstitial capture, (ii) development of very thin sensors, to decrease the amount of leakage current and therefore trapping, and (iii) doping of the gain layer using Carbon.

It has recently been proven [34] that it is possible to maintain the same timing performance of unirradiated UFSD sensors up to fluences of $3 \cdot 10^{14}$ n_{eq}/cm^2, if the detector is cooled to 253 K. The time resolution worsens for fluences of 10^{15} n_{eq}/cm^2, becoming a factor ~ 2 bigger than in the unirradiated case.

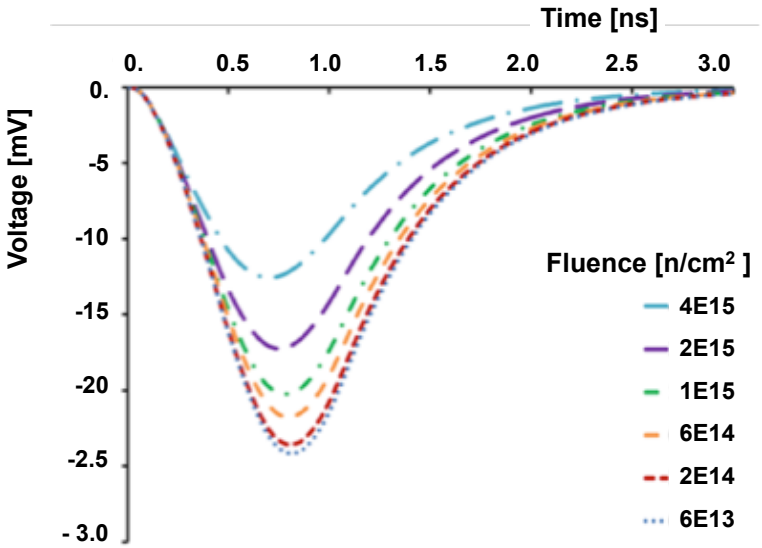

Figure 10. Signal change in a 50 μm silicon sensor as a function of irradiation levels (the only effect considered in this plot is charge trapping).

5 Productions and Performances of Ultra-Fast Silicon Sensors

The first publication containing measurements of LGAD sensors has been presented in 2014 by the Centro Nacional de Microelectrónica (CNM) Barcelona [18] while the first production of thin UFSD (50 μm) by CNM was presented in 2016 [35]. First beam test results on thin UFSD manufactured by CNM have been obtained in 2016 [36]. The Fondazione Bruno Kessler (FBK) has also designed [19], and produced LGAD sensors, up to now only 300 μm thick [37]; the first FBK production of thin LGAD is expected in early 2017. At the 2016 IEEE conference it was announced [38] that Hamamatsu photonics has produced successfully thin UFSD (50 and 80 μm thick) In the past 3 years CNM has manufactured a variety of LGAD designs, exploring different substrates (float zone, silicon-on-insulator, epitaxial with high and medium resistivity), reaching a well-controlled manufacturing capability. FBK has manufactured a single run of very high quality, exploring traditional LGAD design, segmented p-side read-out and AC coupled read-out.

5.1 Results from 50 μm thick UFSD

Thin UFSD produced by CNM were tested at CERN with a 180 GeV/c π-meson beam. Several $1.2 \times 1.2\,\mathrm{mm}^2$ UFSD read-out by a fully custom broadband current amplifier and a trigger board reading a SiPM coupled to a quartz bar were used [36]. This beam test, coupled with complementary laser measurements performed in our laboratories, provides the opportunity to perform detailed studies of the mechanisms governing UFSD time resolution and to compare these measurements to our simulation.

The left side of figure 11 shows typical beam test signals, and the right side shows a comparison between data and WF2, demonstrating the capability of WF2 to reproduce the UFSD beam test signals accurately. The signals are very fast, with low noise and large slew rate, ideal for timing studies. The time resolution of each sensor and that of the SiPM have then been obtained from the

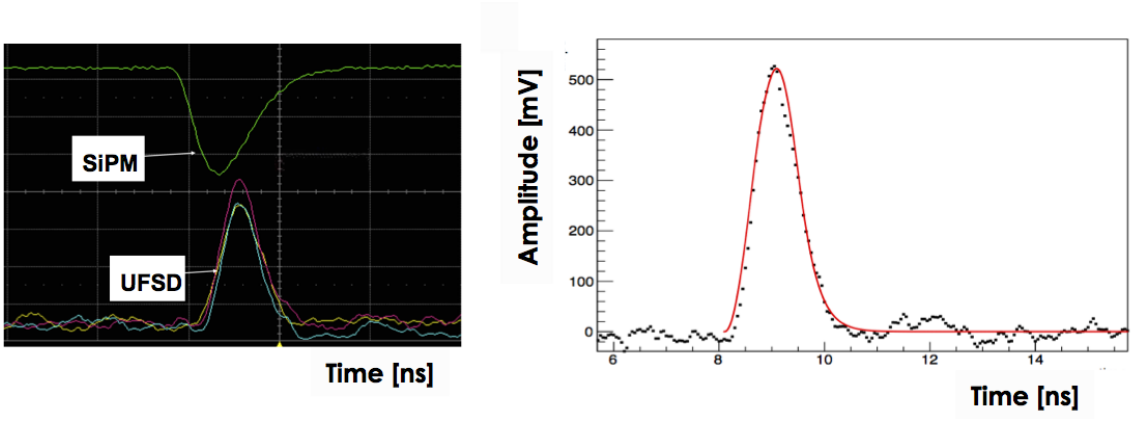

Figure 11. Left: signals of a beam test event showing the coincidence of three 50 μm thick UFSD sensors and the SiPM trigger counter. Right: data (dots) compared to WF2 simulation (solid line).

time differences between pairs of UFSD and between each UFSD and the SiPM. The time resolution of combined UFSD has been evaluated as the difference between the average time of two or three UFSD and the SiPM, table 1. The results of table 1 agree well with the expected $\sigma(N) = 1/\sqrt{N}$ behaviour, demonstrating that the 3 sensors are of equal high quality. The timing resolution of a single UFSD is measured to be 34 ps for 200 V bias and 27 ps for 230 V bias. A system of three UFSD has a measured timing resolution of 20 ps for a bias of 200 V, and 16 ps for a bias of 230 V.

Table 1. Timing resolution for single ($N = 1$), doublet ($N = 2$) and triplets ($N = 3$) of UFSD at bias voltages of 200 V and 230 V.

V bias [V]	200 V	230 V
$\sigma_t(N = 1)$	34.1 ps	27.4 ps
$\sigma_t(N = 2)$	24.2 ps	19.8 ps
$\sigma_t(N = 3)$	19.9 ps	16.4 ps

6 Summary

Tracking in 4 dimensions requires the development of dedicated sensors. The most important features to achieve excellent time resolution are: (i) high field to saturate drift velocity and minimise signal distortion, (ii) geometries as similar as possible to parallel plate capacitors, providing uniform electric and weighting fields, (iii) high velocity carriers, to have large dV/dt, (iv) low capacitance, to minimise jitter and (v) small volumes, to minimise shot noise.

Low-Gain Avalanche Diodes are a novel type of silicon detectors characterised by a controlled, low internal gain, that cross-bred traditional silicon sensors with APD, enjoying the best characteristics of both families. The LGAD thecnology allowed the design of segmented silicon sensors with added timing capabilities, the so-called Ultra-Fast Silicon Detectors, able to achieve a time resolution of $\sigma_t \sim 30$ ps. This results represent the fisrt step towards the development of a full tracker system capable to provide complete 4D information by means of UFSD.

Acknowledgments

We thank our collaborators within RD50, ATLAS and CMS who participated in the development of UFSD. Our special thanks to the technical staff at UC Santa Cruz, INFN Torino, CNM Barcelona and FBK Trento. This work was partially performed within the CERN RD50 collaboration.

The work was supported by the United States Department of Energy, grant DE-FG02-04ER41286. Part of this work has been financed by the European Union Horizon 2020 Research and Innovation funding program, under Grant Agreement no. 654168 (AIDA-2020) and Grant Agreement no. 669529 (ERC UFSD669529), and by the Italian Ministero degli Affari Esteri and INFN Gruppo V.

References

[1] G. Pellegrini et al., *Technology developments and first measurements of Low Gain Avalanche Detectors (LGAD) for high energy physics applications*, *Nucl. Instrum. Meth.* **A765** (2014) 24.

[2] H.F.-W. Sadrozinski, *Exploring charge multiplication for fast timing with silicon sensors*, talk given at the *20th RD50 Workshop*, Bari, Italy, June 2012, http://indico.cern.ch/event/175330/contributions/283780/attachments/225144/315064/RD50_Bari_UFSD_Sadrozinski.pdf.

[3] N. Cartiglia et al., *Design optimization of ultra-fast silicon detectors*, *Nucl. Instrum. Meth.* **A796** (2015) 141.

[4] N. Cartiglia et al., *The 4D pixel challenge*, 2016 *JINST* **11** C12016.

[5] ATLAS upgrade project, https://cds.cern.ch/record/2055248/files/LHCC-G-166.pdf.

[6] CMS upgrade project, https://cds.cern.ch/record/2020886?ln=en&asof=2099-12-31.

[7] *High-Luminosity Large Hadron Collider (HL-LHC): Preliminary Design Report*, CERN-2015-005 (2015).

[8] H. Spieler, *Fast timing methods for semiconductor detectors*, *IEEE Trans. Nucl. Sci.* **NS-29** (1982) 1142.

[9] A. Rivetti, *Fast front-end electronics for semiconductor tracking detectors: Trends and perspectives*, in proceedings of *HSTD9*, Hiroshima, Japan, 2013, *Nucl. Instrum. Meth.* **A765** (2014) 202.

[10] M. Mota and J. Christiansen, *A High-Resolution Time Interpolator Based on a Delay Locked Loop and an RC Delay Line*, *IEEE J. Solid-State Circuits* **34** (1999) 1360.

[11] F. Cenna et al., *Weightfield2: A fast simulator for silicon and diamond solid state detector*, *Nucl. Instrum. Meth.* **A796** (2015) 149.

[12] N. Cartiglia et al., *Tracking in 4 dimensions*, submitted to *Nucl. Instrum. Meth.* **A** (2016).

[13] W. Shockley, *Currents to Conductors Induced by a Moving Point Charge*, *J. Appl. Phys.* **9** (1938) 635.

[14] S. Ramo, *Currents Induced by Electron Motion*, *Proc. IRE* **27** (1939) 584.

[15] E. Martin et al., *Review of results for the NA62 gigatracker read-out prototype*, 2012 *JINST* **7** C03030.

[16] M. Benoit, R. Cardarelli, S. Débieux, Y. Favre, G. Iacobucci, M. Nessi et al., *100 ps time resolution with thin silicon pixel detectors and a SiGe HBT amplifier*, arXiv:1511.04231.

[17] P. Fernandez et al., *Simulation of new p-type strip detectors with trench to enhance the charge multiplication effect in the n-type electrodes*, *Nucl. Instrum. Meth.* **A658** (2011) 98.

[18] G. Pellegrini et al., *Technology developments and first measurements of Low Gain Avalanche Detectors (LGAD) for High Energy Physics applications*, *Nucl. Instrum. Meth.* **A765** (2014) 12.

[19] G.-F. Dalla Betta et al., *Design and TCAD simulation of double-sided pixelated low gain avalanche detectors*, *Nucl. Instrum. Meth.* **A796** (2015) 154.

[20] H.-W. Sadrozinski et al., *Sensors for ultra-fast silicon detectors*, *Nucl. Instrum. Meth.* **A765** (2014) 7.

[21] H.F.W. Sadrozinski et al., *Ultra-fast silicon detectors*, *Nucl. Instrum. Meth.* **A730** (2013) 226.

[22] Hamamatsu Photonics, *Characteristics and use of SiAPD*, Technical Information **SD-28**.

[23] C. Scharf and R. Klanner, *Measurement of the drift velocities of electrons and holes in high-ohmic ⟨100⟩ silicon*, *Nucl. Instrum. Meth.* **A799** (2015) 81 [arXiv:1503.08656].

[24] C.R. Crowell and S.M. Sze, *Temperature dependence of avalanche multiplication in semiconductors*, *Appl. Phys. Lett.* **9** (1966) 242.

[25] R. Mulargia et al., *Temperature dependence of the response of ultra fast silicon detectors*, 2016 *JINST* **11** C12013.

[26] R. Van Overstraeten and H. De Man, *Measurement of the ionization rates in diffused silicon p-n junctions*, *Solid State Electron.* **13** (1970) 583.

[27] D.J. Massey et al., *Temperature dependence of impact ionization in submicrometer silicon devices*, *IEEE Trans. Electron Devices* **53** (2006) 2328.

[28] A.G. Chynoweth, *Ionization rates for electrons and holes in silicon*, *Phys. Rev.* **109** (1958) 1537.

[29] M. Valdinoci et al., *Impact-ionization in silicon at large operating temperature*, in proceedings of *Simulation of Semiconductor Processes and Devices*, Kyoto, 1999, pp. 27–30.

[30] Y. Okuto and C.R. Crowell, *Ionization coefficients in semiconductors: a nonlocalized property*, *Phys. Rev.* **B 10** (1974) 4284.

[31] B. Baldassarri et al., *Signal formation in irradiated silicon detectors*, submitted to *Nucl. Instrum. Meth.* **A** (2016).

[32] G. Kramberger et al., *Radiation effects in Low Gain Avalanche Detectors after hadron irradiations*, 2015 *JINST* **10** P07006.

[33] RD50 collaboration, http://rd50.web.cern.ch/rd50/.

[34] J. Lange et al., *Gain and time resolution of 50 µm LGADs before and after irradiation*, talk given at the *29th RD50 Workshop*, CERN, Switzerland, November 2016, http://indico.cern.ch/event/580875/contributions/2374877/attachments/1375420/2088359/Lange_LGADtimingResults_RD50_November2016.pdf.

[35] M. Carulla et al., *First 50 µm thick LGAD fabrication at CNM for the HGTD and CT-PPS*, talk given at the *28th RD50 Workshop*, Torino, Italy, June 2016, http://agenda.infn.it/getFile.py/access?contribId=20&sessionId=8&resId=0&materialId=slides&confId=11109.

[36] N. Cartiglia et al., *Beam test results of a 16 ps timing system based on ultra-fast silicon detectors*, submitted to *Nucl. Instrum. Meth.* **A** (2016).

[37] A. Staiano, *New Developments in the Design and Production of Low-Gain Avalanche Detectors*, 2016 IEEE, Strasbourg, France, in press.

[38] H. Sadrozinski, *Measurement of the Time Resolution of Ultra-Fast Silicon Detectors (UFSD)*, 2016 IEEE, Strasbourg, France, in press.